Supplementary Information

Oligomeric chain extender-derived anion conducting membrane materials with poly(*p*-phenylene)-based architecture for fuel cells and water electrolyzers

Min Suc Cha[a]†, Ji Eun Park[b]†, Sungjun Kim[c,d]†, Sang-Hun Shin[a], Seok Hwan Yang[a,e], Seung Jae Lee[a,f], Tae-Ho Kim[a], Duk Man Yu[a], Soonyong So[a], Kang Min Oh[g], Yung-Eun Sung[c,d], Yong-Hun Cho[c,g]* and Jang Yong Lee[a]*

† These authors contributed equally to this work;

*Corresponding Authors; yhun00@kangwon.ac.kr (**Y.-H. Cho**); ljylee@krict.re.kr (**J. Y. Lee**)

[a.] Energy Materials Research Center, Korea Research Institute of Chemical Technology (KRICT), Daejeon 34114, Republic of Korea. *E-mail: ljylee@krict.re.kr (J. Y. Lee)

[b.] Department of Energy and Materials Engineering, Dongguk University, Seoul 04620, Republic of Korea.

[c.] Center for Nanoparticle Research, Institute for Basic Science (IBS), Seoul 08826, Republic of Korea.

[d.] School of Chemical and Biological Engineering, Seoul National University, Seoul 08826, Republic of Korea.

[e.] A Department of Chemical Engineering, Hanyang University, Seoul 04763, Republic of Korea.

[f.] A Department of Advanced Material Engineering, Chungbuk National University, Cheongju, 28644, Republic of Korea.

[g.] A Department of Chemical Engineering, Kangwon National University, Samcheok, Gangwon-do 25913, Republic of Korea. *E-mail: yhun00@kangwon.ac.kr (Y.-H. Cho)

1. Supporting Tables

Table S1. Gel permeation chromatography of BrPP-*b*-PSK-w and BrLPP-*b*-PSK-w

Sample	M_n (kg mol^{-1})	M_w (kg mol^{-1})	DPI
BrPP-*b*-PSK-1.5	41.7	109.6	2.63
BrPP-*b*-PSK-2.5	34.0	140.0	4.1
BrPP-*b*-PSK-3.5	40.9	112.0	2.74
BrLPP-*b*-PSK-2.5	40	92.2	2.3
BrLPP-*b*-PSK-3.5	18.1	40.0	2.2

Additional Description: We could not measure the molecular weight of the quaternized polymers using GPC, since the quaternized polymers (QPP-*b*-PSK-w-TMA) were only soluble in DMSO unlike BrPP-*b*-PSK-w and PP-*b*-PSK-w.

Table S2. Activation energies of OH^- and Cl^- anions on QPP-*b*-PSK-w-TMA and FAA-3

Sample	Activation energy (kJ mol^{-1})	
	Cl^- form	OH^- form
QPP-*b*-PSK-1.5-TMA	22.03	14.32
QPP-*b*-PSK-2.5-TMA	20.40	12.76
QPP-*b*-PSK-3.5-TMA	19.52	10.16
FAA-3	26.61	13.16

Table S3. Properties of QPP-*b*-PSK-3.5-Im

Sample	IEC_w^{OH-} (meq. g^{-1})	IEC_w^{Cl-} (meq. g^{-1})	Water uptake (wt%, at 25 °C)	Dimensional Change (%, at 25 °C)			OH- Conductivity (mS cm^{-1})	
				Δl	Δt	ΔV	25 °C	60 °C
QPP-*b*-PSK-3.5-Im	2.0	1.9	38	4	21	31	27	63

Table S4. Performance of state-of-the-art AEMs and PGM-based AEMFC in this work and recent literature.[1-13]

AEMs	AEIs	Anode (Loading, mg_{PGM} cm^{-2})	Cathode (Loading, mg_{PGM} cm^{-2})	Total PGM loading (mg_{PGM} cm^{-2})	Specific Power (W mg_{PGM}^{-1})	Peak Power Density (W cm^{-2})	Cell temperature (°C)	Operating condition (Back pressure / bar)	Ref.
QPP-*b*-PSK-3.5-TMA	**QPC-TMA**	**PtRu/C (0.2)**	**Pt/C (0.1)**	**0.3**	**4.90**	**1.47**	**80**	**H_2-O_2 (1.5/1.5)**	**This work**
QPP-*b*-PSK-3.5-TMA	**QPC-TMA**	**PtRu/C (0.2)**	**Pt/C (0.1)**	**0.3**	**3.03**	**0.91**	**80**	**H_2-Air (1.5/1.5)**	**This work**
QPP-*b*-PSK-3.5-TMA	**QPC-TMA**	**PtRu/C (0.4)**	**Pt/C (0.2)**	**0.6**	**3.02**	**1.81**	**80**	**H_2-O_2 (1.5/1.5)**	**This work[a]**
QPP-*b*-PSK-3.5-TMA	**QPC-TMA**	**PtRu/C (0.4)**	**Pt/C (0.4)**	**0.8**	**2.43**	**1.94**	**75**	**H_2-O_2 (1.0/1.0)**	**This work**
QPP-*b*-PSK-3.5-TMA	**QPC-TMA**	**PtRu/C (0.4)**	**Pt/C (0.4)**	**0.8**	**1.66**	**1.33**	**75**	**H_2-Air (1.0/1.0)**	**This work**
RG-HDPE	RG-BTMA-ETFE	PtRu/C (0.125)	Fe-N-C (1.0)	0.125	10.40	1.3	80	H_2-O_2 (0.0/1.0)	1
RG-HDPE	RG-BTMA-ETFE	PtRu/C (0.6)	Fe-N-C (1.0)	0.6	3.42	2.05	80	H_2-O_2 (2.0/2.0)	1
PDTP-25	PFBP	PtRu/C (0.39)	Pt/C (0.26)	0.65	3.97	2.58	80	H_2-O_2 (1.3/1.3)	2
PDTP-25	PFBP	PtRu/C (0.39)	Pt/C (0.26)	0.65	2.12	1.38	80	H_2-Air (1.3/1.3)	2
PFTP-13	PFBP	Pt/C (0.33)	Pt/C (0.33)	0.66	2.73	1.8	80	H_2-O_2 (1.5/1.5)	3
PFTP-13	PFBP	PtRu/C (0.42)	Pt/C (0.33)	0.75	3.12	2.34	80	H_2-O_2 (1.3/1.3)	3
QPC-TMA	QPC-TMA	PtRu/C (0.4)	Pt/C (0.4)	0.8	2.01	1.61	60	H_2-O_2 (0.0/0.0)	4
PNB	PNB	PtRu/C (0.7)	Pt/C (0.6)	1.3	2.46	3.2	80	H_2-O_2 (0.0/2.0)	5
PNB	PNB	PtRu/C (0.7)	Pt/C (0.6)	1.3	2.08	2.7	80	H_2-O_2 (0.0/2.0)	5
PNB	PNB	PtRu/C (0.7)	Pt/C (0.6)	1.3	1.35	1.75	80	H_2-Air (0.0/2.0)	5
PAP-TP	PAP-BP	PtRu/C (0.15)	Ag/C (1.0)	0.15	6.13	0.92	95	H_2-Air (2.5/1.3)	6
RG-HDPE	RG-BTMA-ETFE	PtRu/C (0.6)	Ag/C (0.85)	0.6	2.87	1.72	80	H_2-O_2 (0.0/0.0)	7
RG-HDPE	RG-BTMA-ETFE	PtRu/C (0.6)	Pt/C (0.4)	1	2.55	2.55	80	H_2-O_2 (0.0/0.0)	7
RG-LDPE	RG-BTMA-ETFE	PtRu/C (0.6)	Pt/C (0.4)	1	2.01	2.01	80	H_2-O_2 (0.0/0.0)	7
m-TPN	TEA-o-BTN	Pt/C (0.6)	Pt/C (0.6)	1.2	1.29	1.55	80	H_2-O_2 (1.5/1.5)	8
PNB	RG-BTMA-ETFE	PtRu/C (0.7)	Pt/C (0.6)	1.3	2.69	3.5	80	H_2-O_2 (0.5/1.0)	9
PNB	RG-BTMA-ETFE	PtRu/C (0.7)	Pt/C (0.6)	1.3	0.92	1.2	80	H_2-Air (0.5/1.0)	9
PNB	RG-BTMA-ETFE	PtRu/C (0.7)	Pt/C (0.6)	1.3	2.59	3.37	80	H_2-O_2 (0.0/0.0)	10
PNB	RG-BTMA-ETFE	PtRu/C (0.7)	Pt/C (0.6)	1.3	2.52	3.27	80	H_2-O_2 (0.0/0.0)	10
PNB	RG-BTMA-ETFE	PtRu/C (0.7)	Pt/C (0.6)	1.3	2.35	3.06	80	H_2-O_2 (0.0/0.0)	10
PNB	RG-BTMA-ETFE	PtRu/C (0.7)	Pt/C (0.6)	1.3	2.31	3	80	H_2-O_2 (0.0/0.0)	10

PAP-TP	PAP-TP	PtRu/C (0.1)	Pt/C (0.4)	0.5	3.32	1.66	80	H_2-O_2 (2.0/2.0)	[11]
PAP-TP	PAP-TP	Pt/C (0.1)	Pt/C (0.4)	0.5	3.08	1.54	80	H_2-O_2 (2.0/2.0)	[11]
PAP-TP	PAP-TP	PtRu/C (0.4)	Pt/C (0.4)	0.8	2.60	2.08	80	H_2-O_2 (2.0/2.0)	[11]
PAP-TP	PAP-TP	Pt/C (0.4)	Pt/C (0.4)	0.8	2.40	1.92	80	H_2-O_2 (2.0/2.0)	[11]
PAP-TP	PAP-TP	PtRu/C (0.6)	Pt/C (0.4)	1	1.45	1.45	80	H_2-O_2 (1.0/1.0)	[12]
TPN	FNL	PtRu/C (0.15)	Pt/C (0.6)	0.75	1.33	1	80	H_2-O_2 (2.85/2.85)	[13]
TPN	FNL	PtRu/C (0.75)	Pt/C (0.6)	1.35	1.08	1.46	80	H_2-O_2 (2.85/2.85)	[13]
TPN	FNL	PtRu/C (0.75)	Pt/C (0.6)	1.35	0.50	0.68	80	H_2-Air (2.85/2.85)	[13]
FAA-3	QPC-TMA	PtRu/C (0.2)	Pt/C (0.1)	0.3	2.97	0.89	75	H_2-O_2 (1.0/1.0)	This work
FAA-3	QPC-TMA	PtRu/C (0.4)	Pt/C (0.2)	0.6	2.28	1.37	75	H_2-O_2 (1.0/1.0)	This work
FAA-3	QPC-TMA	PtRu/C (0.4)	Pt/C (0.4)	0.8	1.96	1.57	75	H_2-O_2 (1.0/1.0)	This work
FAA-3	QPC-TMA	PtRu/C (0.4)	Pt/C (0.4)	0.8	1.43	1.14	75	H_2-Air (1.0/1.0)	This work

[a] Figure S17

Table S5. The summary of AEMWE performance using commercial and synthesized membranes reported in literature[14-24] and performed in this work.

AEMs	Catalyst (Anode/Cathode)	Loading (mg cm^{-2})	Temperature (°C)	Performance at 1.9 V (A cm^{-2})	Ref.
QPP-*b*-PSK-3.5-TMA	**NiFe / Pt/C**	**1.0 / 0.4**	**90**	**4.000**	**This work**
QPP-*b*-PSK-3.5-TMA	**NiFe / Pt/C**	**1.0 / 0.4**	**80**	**3.750**	**This work**
QPP-*b*-PSK-3.5-TMA	**IrO_2 / Pt/C**	**2.0 / 0.4**	**80**	**3.150**	**This work**
A201 (Tokuyama Co.)	IrO_2 / Pt	2.9 / 3.2	50	0.520	[14]
QPPO	$NiCo_2O_4$ / Pt/C	8 / 0.3	70	0.950	[15]
PPO-24-BIM	IrO_2 / Pt/C	3 / 1.5	50	0.400	[16]
FAA-3-50 (Fumatech Co.)	g-cn-cnf / Pt/C	6 / 0.4	60	0.734	[17]
FAA-3PE-30 (Fumatech Co.)	$Ni_{90}Fe_{10}/CeO_2$ NPs / Pt/C	6 / 1	50	1.950	[18]
FAA-3-50 (Fumatech Co.)	IrO_2 / Pt/C	2 / 0.4	70	1.500	[19]
PAEK-APMBI	Ni foam	-	60	0.500	[20]
Aemion (Ionomr Innovations Inc.)	Ir / Pt/C	3.5 / 1	50	1.900	[21]
PISPVA46	IrO_2 / Pt/C	2 / 0.5	60	0.450	[22]
X37-50 Grade T (Dioxide materials Co.)	CuCo oxide / Pt/C	3.8 / 1	45	2.100	[23]
PFOTFPH-TMA	IrO_2 / Pt/C	1.2 / 0.3	80	1.500	[24]

2. Supporting Scheme

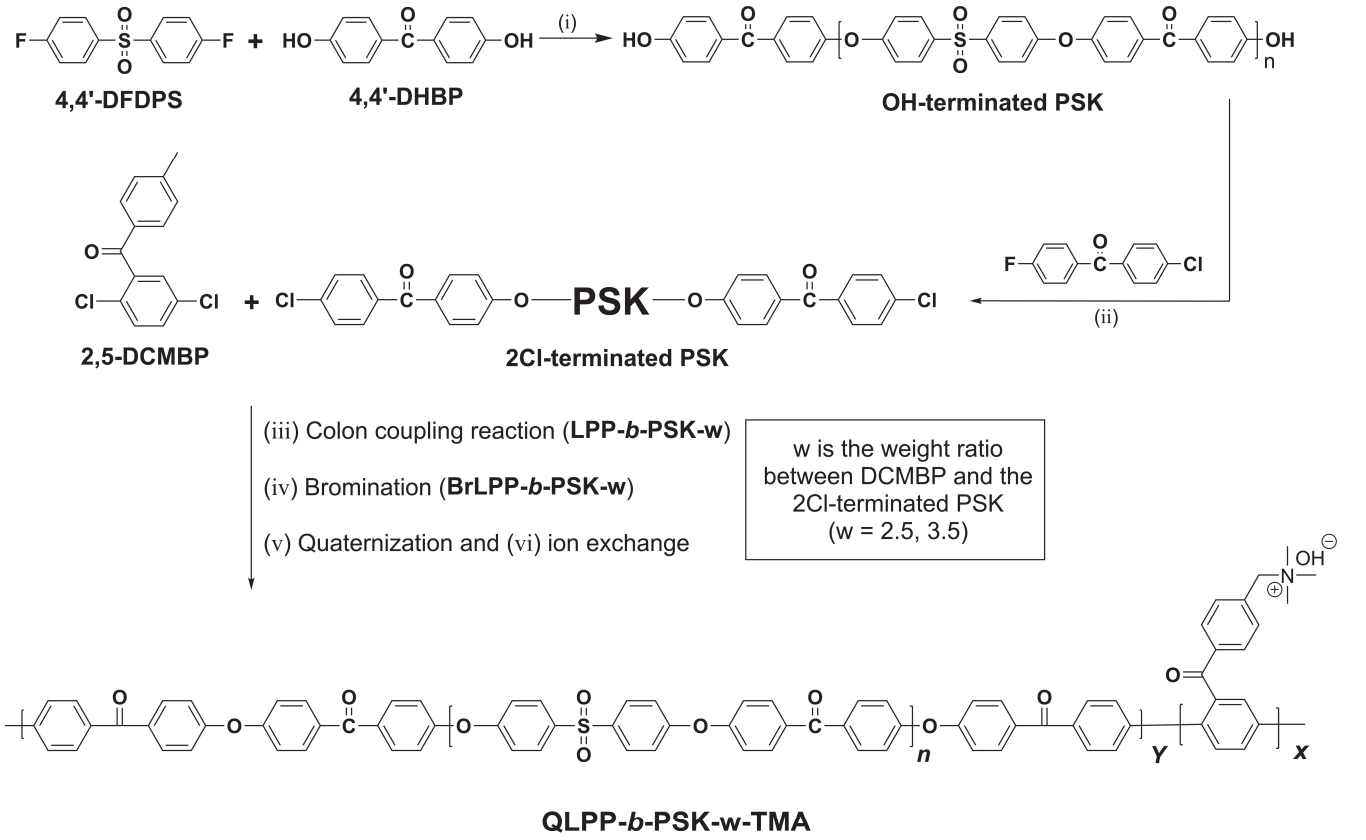

Scheme S1. Synthetic procedure of QLPP-*b*-PSK-w-TMA. The reaction agent, solvent and condition for each steps (form i to vi) to synthesize QLPP-*b*-PSK-w-TMA are as follow ; (i) K_2CO_3, DMAc 165 °C for 16h (ii) K_2CO_3, DMAc, 130 °C for 16h (iii) $NiBr_2$, TPP, Zinc, DMAc, 80 °C for 16h (iv) NBS, TCE, 90 °C for 24h (v) 45 wt% TMA solution, 25 °C for 24h (vi) immersed in 1M KOH at room temperature for 24h.

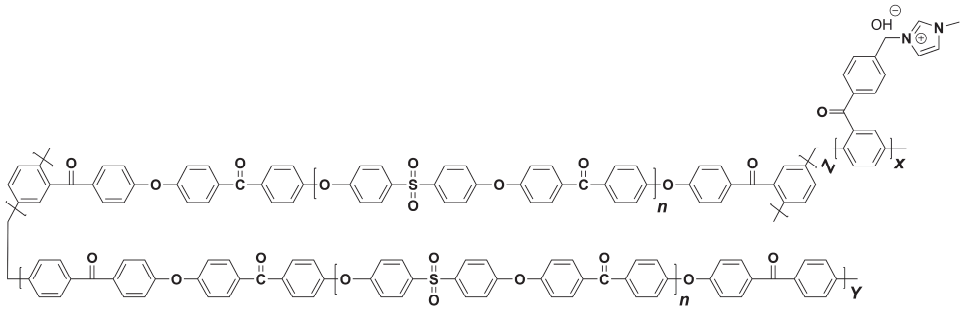

Scheme S2. Chemical structure of QPP-*b*-PSK-3.5-Im

3. Supporting Figures

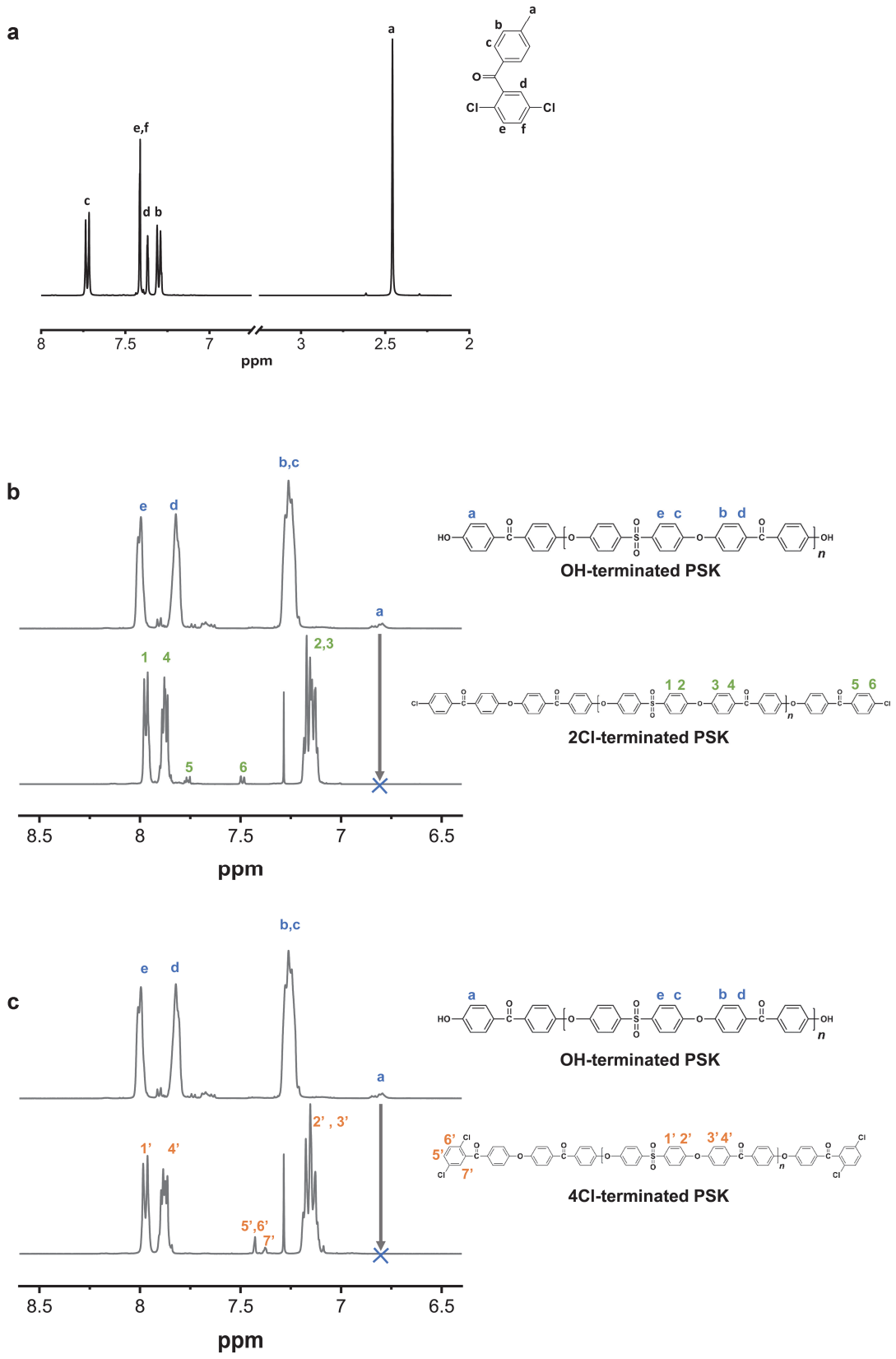

Figure S1.^{1}H NMR spectrum of monomer and oligomers : (a) DCMBP, (b) 2Cl-terminated PSK and (c) 4Cl-terminated PSK

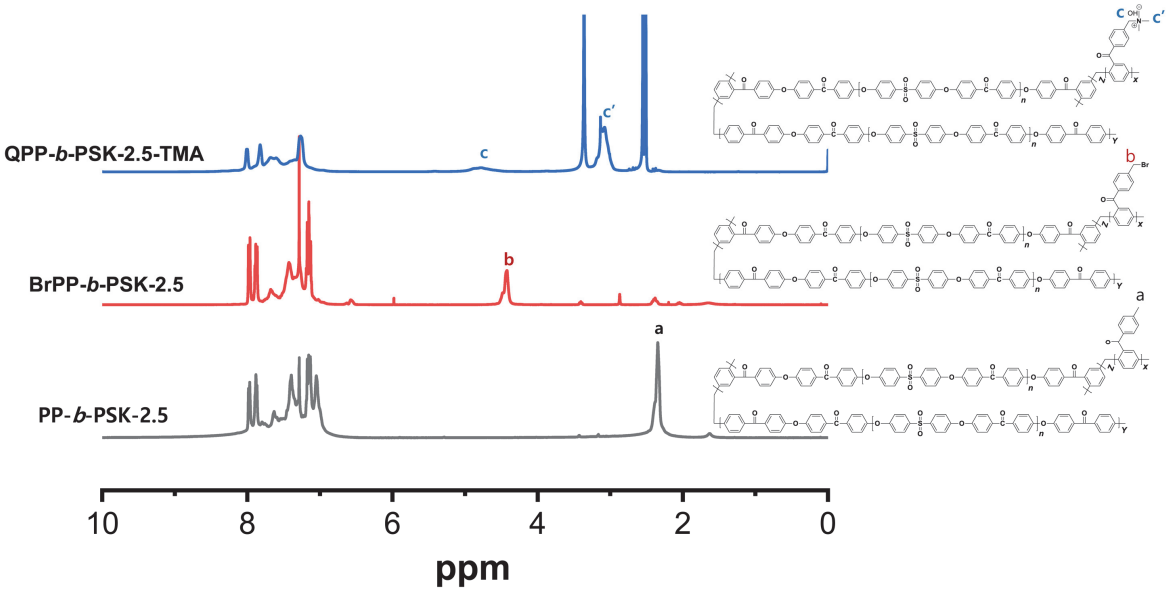

Figure S2. ^{1}H NMR spectrum of QPP-*b*-PSK-w-TMA. (From top to bottom: PP-b-PSK-2.5, BrPP-b-PSK-2.5, QPP-*b*-PSK-2.5)

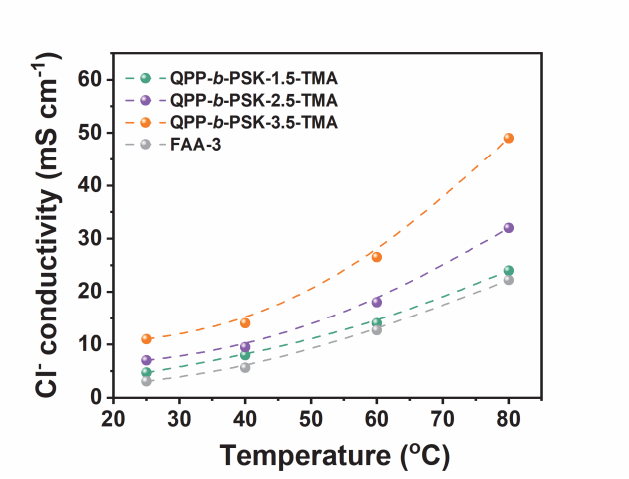

Figure S3. Cl^- ion conductivity of QPP-*b*-PSK-w-TMA and FAA-3

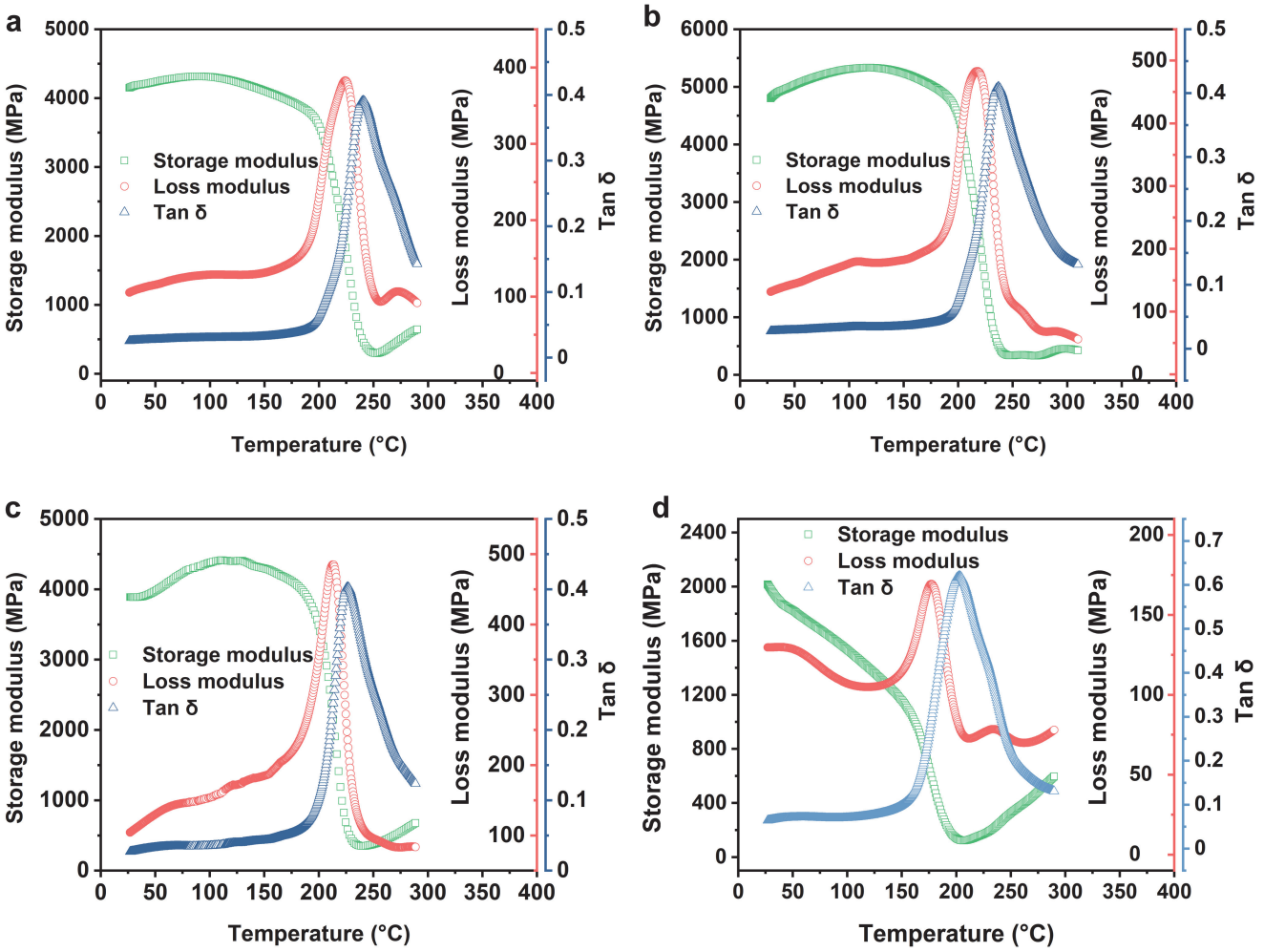

Figure S4. Dynamic mechanical analysis (DMA) curves of QPP-*b*-PSK-w-TMA: (a) QPP-*b*-PKS-1.5-TMA, (b) QPP-*b*-PKS-2.5-TMA, (c) QPP-*b*-PKS-3.5-TMA and (d) FAA-3)

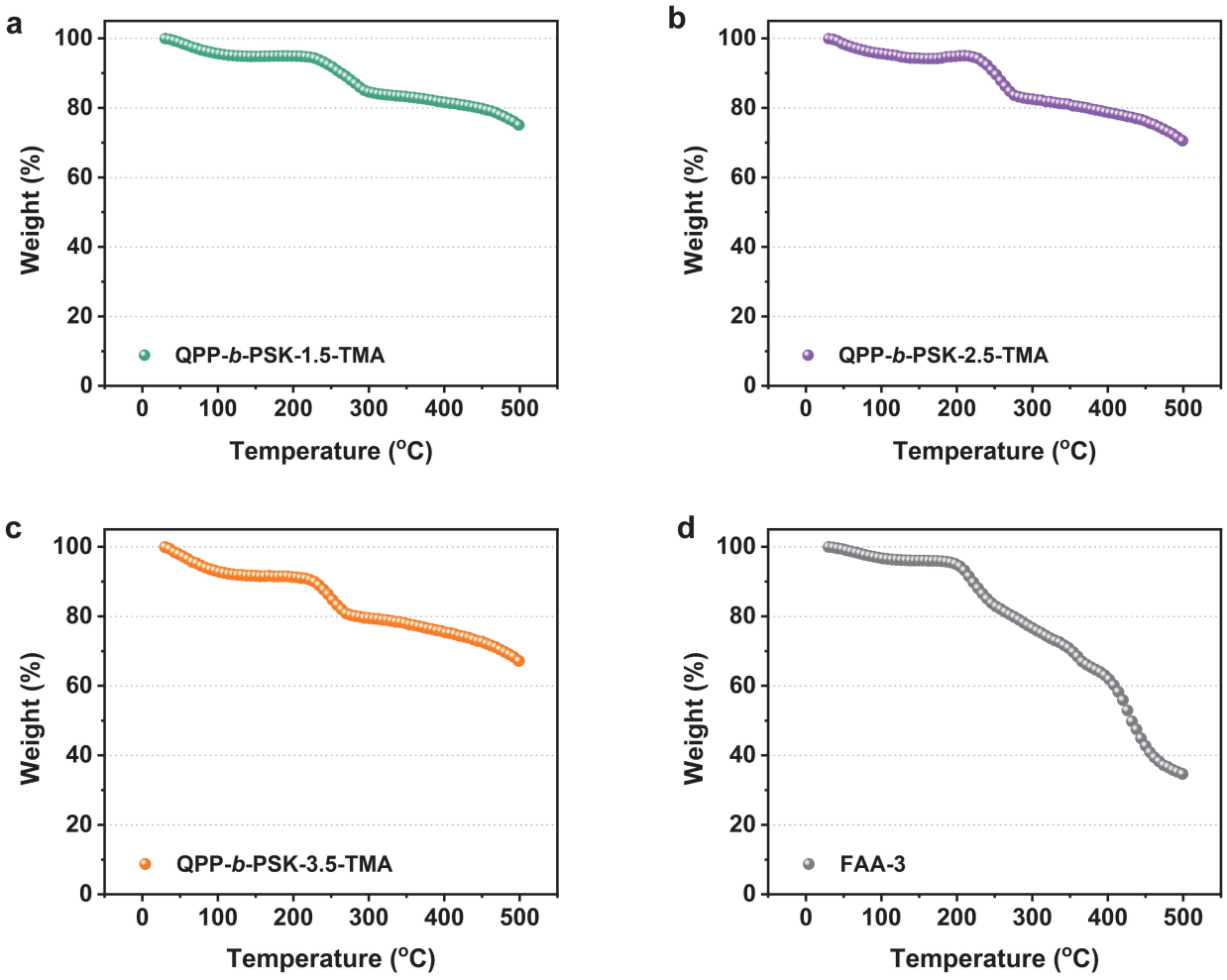

Figure S5. TGA curves of QPP-*b*-PSK-w-TMA and FAA-3 : (a) QPP-*b*-PSK-1.5-TMA, (b) QPP-*b*-PSK-2.5-TMA, (c) QPP-*b*-PSK-3.5-TMA, (d) FAA-3

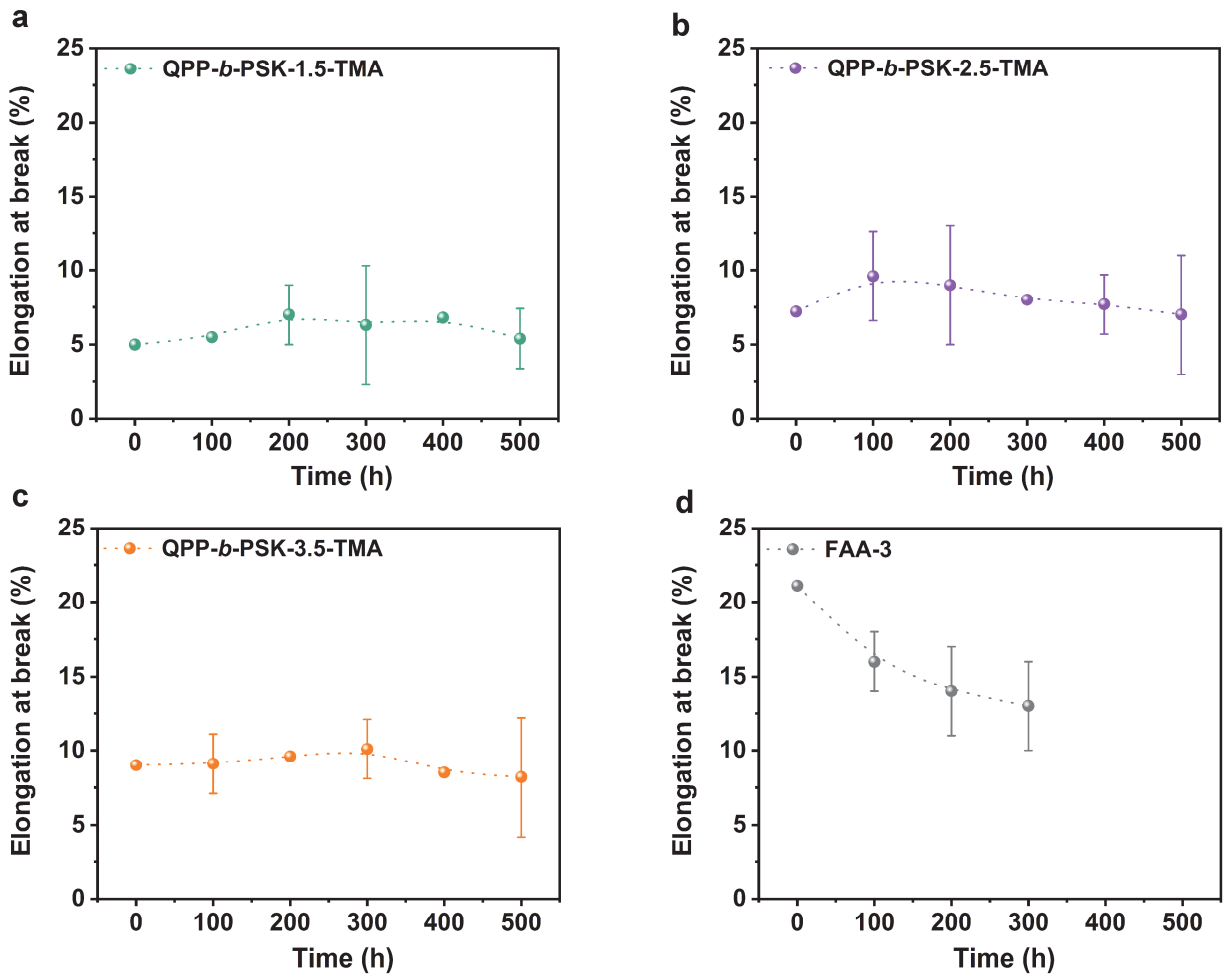

Figure S6. Ion exchange capacity change of QPP-*b*-PSK-w-TMA and FAA-3 during the alkaline stability test under 1 M KOH solution at 80 °C : (a) QPP-*b*-PSK-1.5-TMA, (b) QPP-*b*-PSK-2.5-TMA, (c) QPP-*b*-PSK-3.5-TMA, (d) FAA-3

Sample	Immersed in 1M KOH solution		Sample	Immersed in 3M KOH solution	
	bended	twisted		bended	twisted
QPP-*b*-PSK-1.5-TMA			QPP-*b*-PSK-1.5-TMA	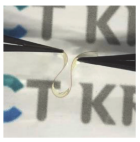	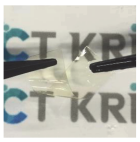
QPP-*b*-PSK-2.5-TMA	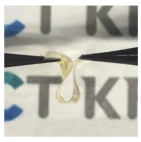		QPP-*b*-PSK-2.5-TMA		
QPP-*b*-PSK-3.5-TMA		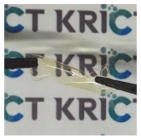	QPP-*b*-PSK-3.5-TMA		
QPP-*b*-PSK-3.5-Im			QPP-*b*-PSK-3.5-Im	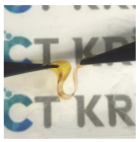	

Figure S7. Digital photo of QPP-*b*-PSK-w-TMA and QPP-*b*-PSK-3.5-Im after chemical stability test under 1M (left) or 3M (right) KOH solution at 80 ℃

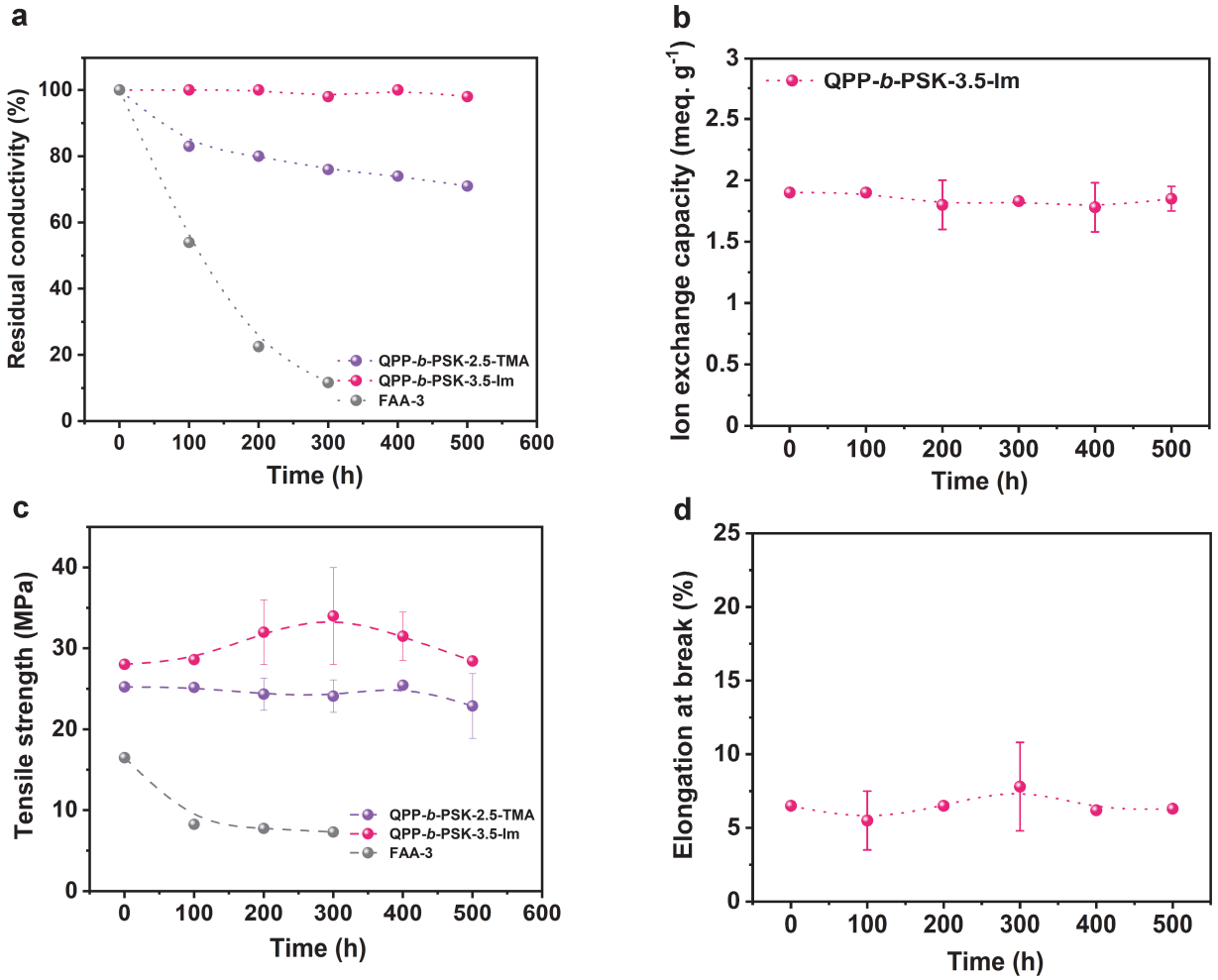

Figure S8. Alkaline stability test investigated by immersing QPP-*b*-PSK-3.5-Im in 1 M KOH solution at 80 °C for 500 h. (a) Residual conductivity, (b) IEC changes and (c), (d) mechanical properties changes ((c) tensile strength, (d) elongation at break).

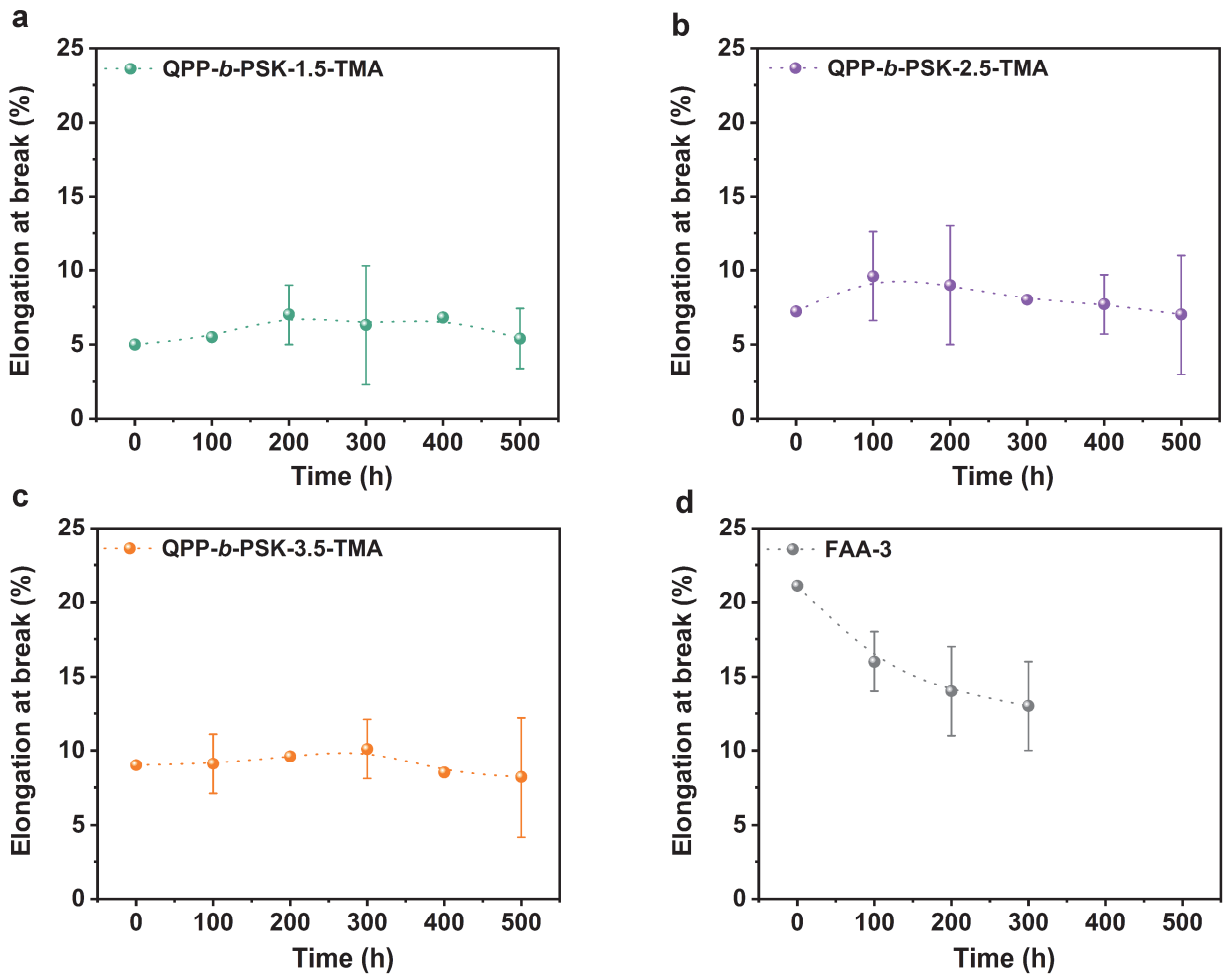

Figure S9. Elongation change of QPP-*b*-PSK-w-TMA and FAA-3 as a function of alkaline exposure time : (a) QPP-*b*-PSK-1.5-TMA, (b) QPP-*b*-PSK-2.5-TMA, (c) QPP-*b*-PSK-3.5-TMA, (d) FAA-3

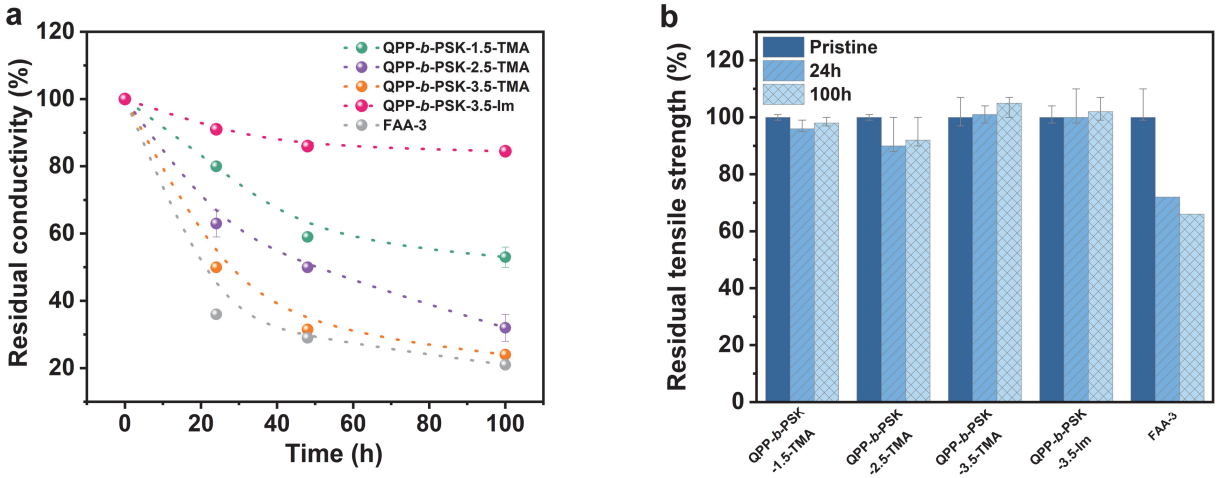

Figure S10. Alkaline stability test investigated by immersing the synthesized membrane in 3 M KOH solution at 80 °C for 100 h. (a) Residual conductivity and (b) mechanical properties changes of QPP-*b*-PSK-w-TMA, QPP-*b*-PSK-3.5-Im and FAA-3.

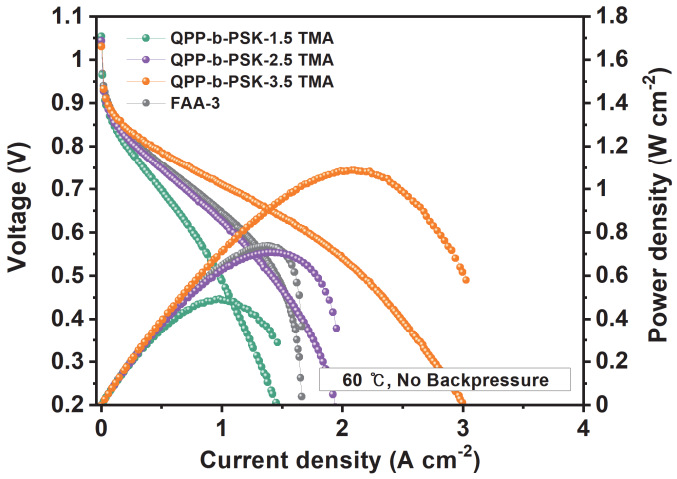

Figure S11. Single cell performance of AEMFCs with QPP-*b*-PSK-w-TMA (w = 1.5, 2.5, and 3.5) and FAA-3 AEMs with FAA-3 ionomer.

Testing conditions: 60 wt.% PtRu/C and Pt/C catalysts were used in the anode and cathode, respectively, and the catalyst loadings of both electrodes were fixed at 0.4 mg_{PGM} cm^{-2}. The temperature of the cell was maintained at 60 °C. Flow rates of humidified hydrogen (dew point of 56 °C) and oxygen (dew point of 58 °C) were 0.8 and 1.0 L min^{-1}, respectively.

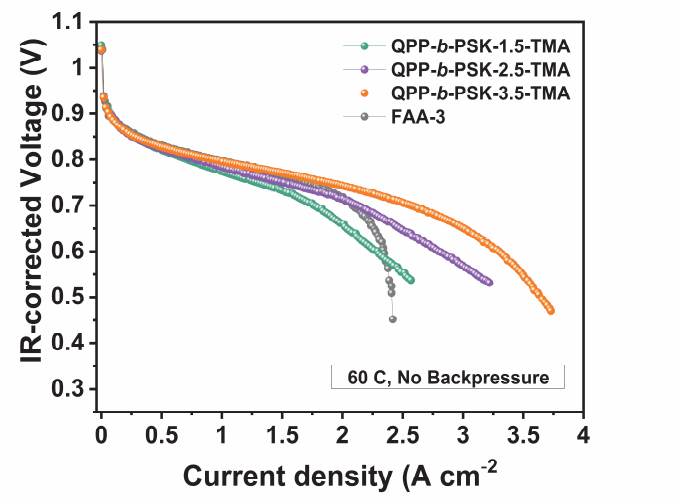

Figure S12. iR-corrected polarization curves of AEMFCs with different AEMs (QPP-b-PSK-w-TMAs, and FAA-3).

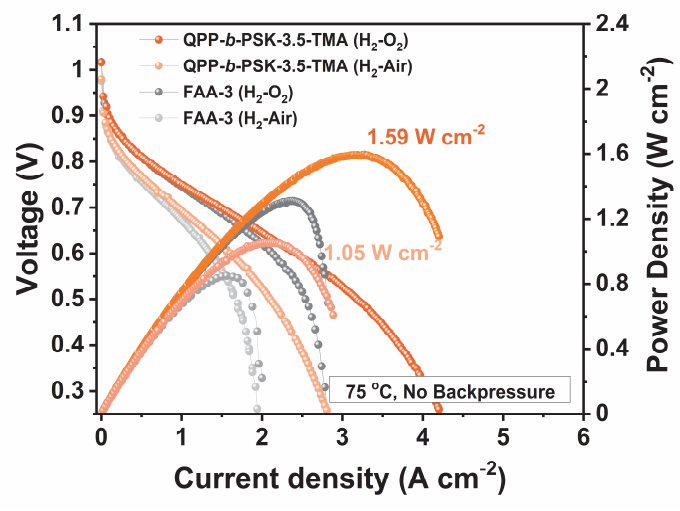

Figure S13. Single-cell performance of the AEMFCs using QPP-*b*-PSK-3.5-TMA or FAA-3 AEMs with QPC-TMA ionomer at high temperature of 75 °C.[4] 60 wt.% PtRu/C and Pt/C catalysts were used in the anode and cathode, respectively, and the catalyst loadings of both electrodes were fixed at 0.4 mg_{PGM} cm^{-2}. The temperature of the cell was maintained at 75 °C. The flow rates of humidified hydrogen (dew point of 69 °C) and oxygen or air (dew point of 73 °C) were 0.8 and 1.0 L min^{-1} without any back-pressure, respectively.

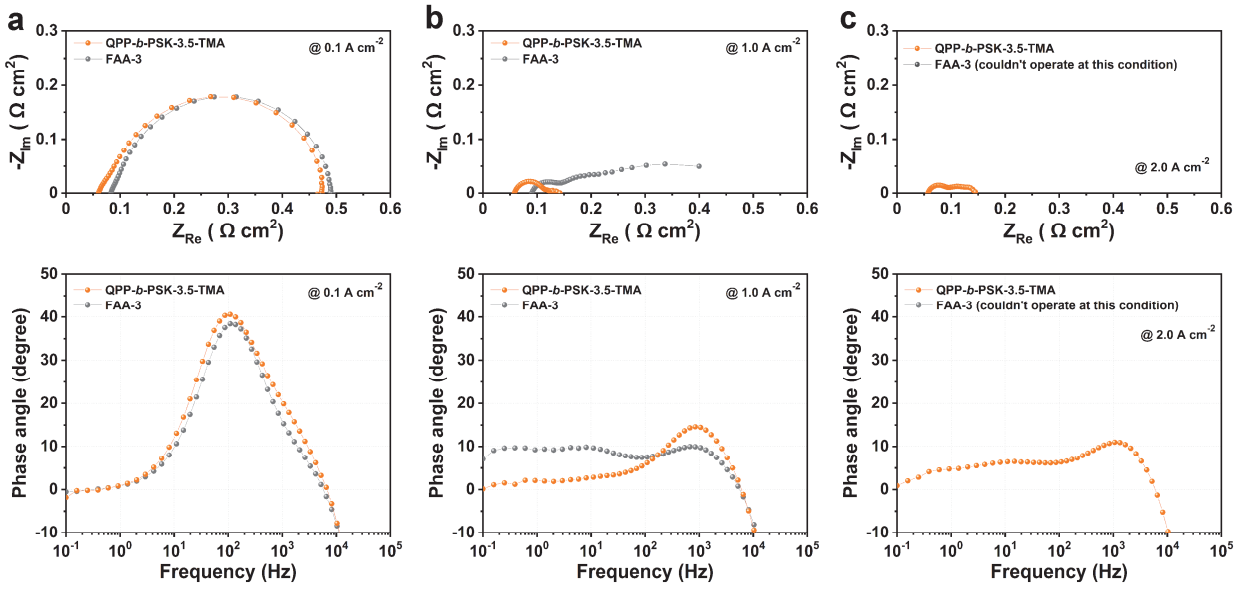

Figure S14. Nyquist and Bode plots of EIS spectra of the low PGM-loaded AEMFCs using QPP-b-PSK-3.5-TMA or FAA-3 membranes with QPC-TMA ionomer measured at different current densities: (a) 0.1 A cm^{-2} (b) 1.0 A cm^{-2}, and (c) 2.0 A cm^{-2}. Testing conditions are the same as cell performance evaluation conditions.

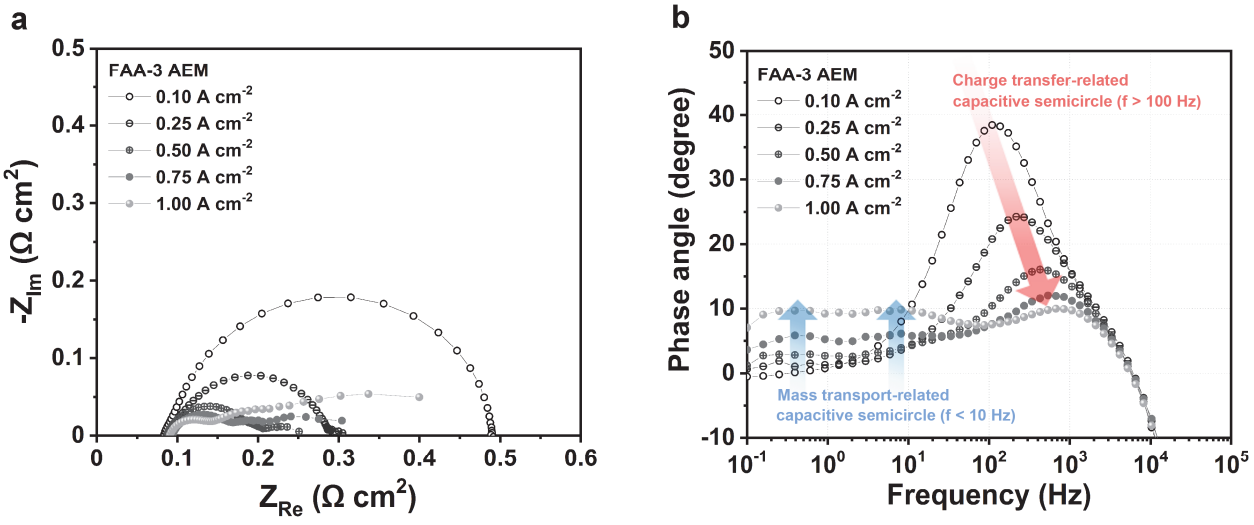

Figure S15. EIS spectra of the low PGM-loaded AEMFC using FAA-3 membrane with QPC-TMA ionomer measured at different current densities (a) Nyquist plot and (b) Bode-phase angle plot. Testing conditions are the same as cell performance evaluation conditions.

Additional Description: As shown in **Figure S15**, at a low current density of 0.1 A cm^{-2}, there is only the capacitive semicircle with a high peak frequency (f_p) of about 100 Hz. This high frequency arc could be related to the charge transport process within the electrodes of the cell because its size and the peak frequency of the arc decreased and increased, respectively, as the current density increased. On the other hand, at much higher current density over 0.75 A cm^{-2}, there are noticeable capacitive semicircles with much lower peak frequency (f_p < 10 Hz) compared to the high frequency semicircle (f_p > 100 Hz). From the fact that the size of these arcs increases with current density, it can be inferred that the low frequency arcs are closely related to the mass transport process in the system.

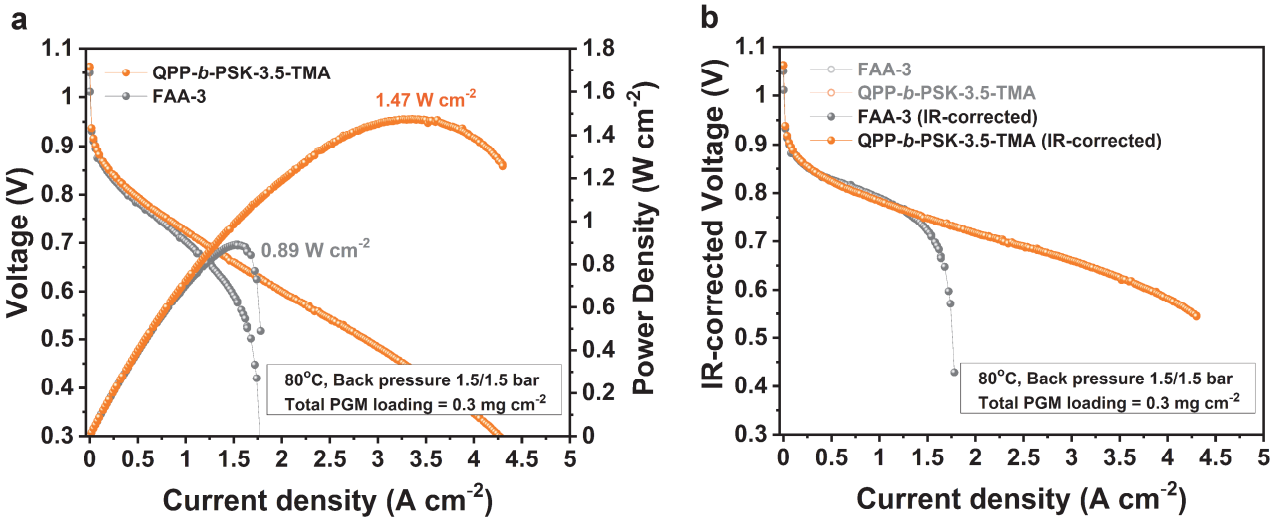

Figure S16. (a) Single cell polarization and (b) iR-corrected polarization curves of AEMFCs with different AEMs (QPP-b-PSK-3.5-TMA, and FAA-3).

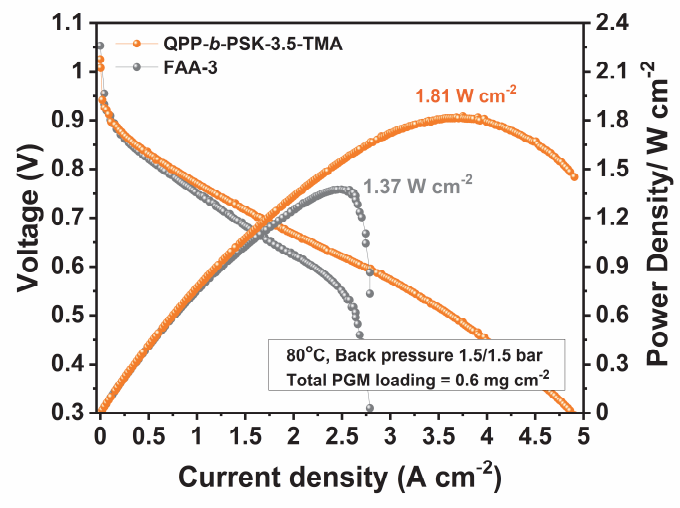

Figure S17. Single-cell polarization curves of the 0.6 mg_{PGM} cm^{-2} loaded AEMFCs using QPP-*b*-PSK-3.5-TMA or FAA-3 AEMs with QPC-TMA Ionomer. Anode catalyst: 60 wt.% PtRu/C with PGM loading of 0.4 mg_{PGM} cm^{-2}. Cathode catalyst: 40 wt.% Pt/C with PGM loading of 0.2 mg_{PGM} cm^{-2}

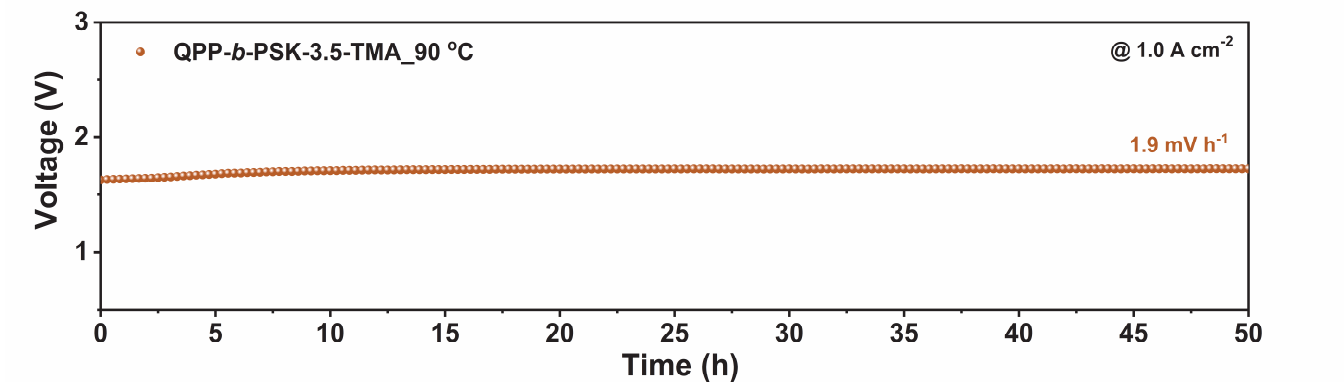

Figure S18. Durability tests of QPP-*b*-PSK-3.5-TMA_90 °C at a constant current density of 1.0 A cm^{-2}. The QPP-*b*-PSK-3.5-TMA_90 was evaluated for 50 h. The NiFe with the loading of 1 mg cm^{-2} and 40 wt. % Pt/C with the loading of 0.4 mg cm^{-2} were employed in the anode and cathode, respectively. The AEMWEs were operated under 1M KOH-feeding method.

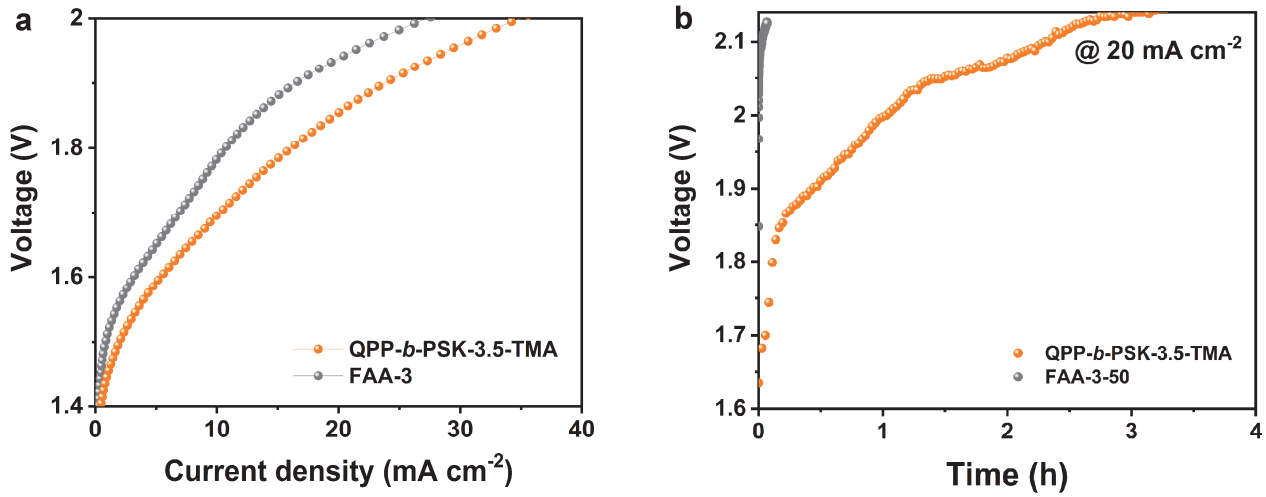

Figure S19. Performance and stability of AEMWEs operated using pure water method. (a) Polarization curves of QPP-*b*-PSK-3.5-TMA and FAA-3 AEMWEs using pure water method. (b) Stability test performed at a constant current density of 20 mA cm^{-2}. The NiFe and 40 wt.% Pt/C catalyst were used in anode and cathode, respectively. The catalyst loadings in anode and cathode were 1.0 and 0.4 mg cm^{-2}. The temperature was maintained at 80 °C.

4. References

1. A. S. Horie Adabi, Noor Ul Hassan, John R. Varcoe, Barr Zulevi, Alexey Serov, John R. Regalbuto, and William E. Mustain, *Nat. Energy*, 2021, **6**, 834–843
2. N. Chen, C. Hu, H. H. Wang, S. P. Kim, H. M. Kim, W. H. Lee, J. Y. Bae, J. H. Park and Y. M. Lee, *Angew. Chem. Int. Ed.*, 2021, **60**, 7710-7718.
3. N. Chen, H. H. Wang, S. P. Kim, H. M. Kim, W. H. Lee, C. Hu, J. Y. Bae, E. S. Sim, Y. C. Chung, J. H. Jang, S. J. Yoo, Y. Zhuang and Y. M. Lee, *Nat Commun*, 2021, **12**, 2367.
4. M. S. Cha, J. E. Park, S. Kim, S.-H. Han, S.-H. Shin, S. H. Yang, T.-H. Kim, D. M. Yu, S. So, Y. T. Hong, S. J. Yoon, S.-G. Oh, S. Y. Kang, O.-H. Kim, H. S. Park, B. Bae, Y.-E. Sung, Y.-H. Cho and J. Y. Lee, *Energy Environ. Sci.*, 2020, **13**, 3633-3645.
5. N. Ul Hassan, M. Mandal, G. Huang, H. A. Firouzjaie, P. A. Kohl and W. E. Mustain, *Adv. Energy Mater.*, 2020, **10**, 2001986.
6. J. Wang, Y. Zhao, B. P. Setzler, S. Rojas-Carbonell, C. Ben Yehuda, A. Amel, M. Page, L. Wang, K. Hu, L. Shi, S. Gottesfeld, B. Xu and Y. Yan, *Nat. Energy*, 2019, **4**, 392-398.
7. L. Wang, X. Peng, W. E. Mustain and J. R. Varcoe, *Energy Environ. Sci.*, 2019, **12**, 1575-1579.
8. E. J. Park, S. Maurya, A. S. Lee, D. P. Leonard, D. Li, J. Y. Jeon, C. Bae and Y. S. Kim, *J. Mater. Chem. A*, 2019, **7**, 25040-25046.
9. M. Mandal, G. Huang, N. U. Hassan, X. Peng, T. Gu, A. H. Brooks-Starks, B. Bahar, W. E. Mustain and P. A. Kohl, *J. Electrochem. Soc.*, 2020, **167**, 054501.
10. G. Huang, M. Mandal, X. Peng, A. C. Yang-Neyerlin, B. S. Pivovar, W. E. Mustain and P. A. Kohl, *J. Electrochem. Soc.*, 2019, **166**, F637-F644.
11. Q. Li, H. Peng, Y. Wang, L. Xiao, J. Lu and L. Zhuang, *Angew. Chem. Int. Ed.*, 2019, **58**, 1442-1446.
12. H. Peng, Q. Li, M. Hu, L. Xiao, J. Lu and L. Zhuang, *J. Power Sources*, 2018, **390**, 165-167.
13. S. Maurya, S. Noh, I. Matanovic, E. J. Park, C. Narvaez Villarrubia, U. Martinez, J. Han, C. Bae and Y. S. Kim, *Energy Environ. Sci.*, 2018, **11**, 3283-3291.
14. Y. Leng, G. Chen, A. J. Mendoza, T. B. Tighe, M. A. Hickner and C.-Y. Wang, *J. Am. Chem. Soc.*, 2012, **134**, 9054-9057.
15. J. Schauer, J. Hnát, L. Brožová, J. Žitka and K. Bouzek, *J. Membr. Sci*, 2015, **473**, 267-273.
16. A. Marinkas, I. Struźyńska-Piron, Y. Lee, A. Lim, H. S. Park, J. H. Jang, H.-J. Kim, J. Kim, A. Maljusch, O. Conradi and D. Henkensmeier, *Polymer*, 2018, **145**, 242-251.
17. J. E. Park, M.-J. Kim, M. S. Lim, S. Y. Kang, J. K. Kim, S.-H. Oh, M. Her, Y.-H. Cho and Y.-E. Sung, *Appl. Catal. B: Environ.*, 2018, **237**, 140-148.
18. E. Cossar, A. Oyarce Barnett, F. Seland and E. A. Baranova, *Catalysts*, 2019, **9**, 814.
19. J. E. Park, S. Y. Kang, S.-H. Oh, J. K. Kim, M. S. Lim, C.-Y. Ahn, Y.-H. Cho and Y.-E. Sung, *Electrochim. Acta*, 2019, **295**, 99-106.
20. D. D. Tham and D. Kim, *J. Membr. Sci*, 2019, **581**, 139-149.
21. P. Fortin, T. Khoza, X. Cao, S. Y. Martinsen, A. Oyarce Barnett and S. Holdcroft, *J. Power Sources*, 2020, **451**, 227814.
22. H. J. Park, S. Y. Lee, T. K. Lee, H.-J. Kim and Y. M. Lee, *J. Membr. Sci*, 2020, **611**, 118355.
23. Y. S. Park, J. Yang, J. Lee, M. J. Jang, J. Jeong, W.-S. Choi, Y. Kim, Y. Yin, M. H. Seo, Z. Chen and S. M. Choi, *Appl. Catal. B: Environ.*, 2020, **278**, 119276.
24. R. Soni, S. Miyanishi, H. Kuroki and T. Yamaguchi, *ACS Appl. Energy Mater.*, 2021, **4**, 1053-1058.

